

The modulation structure induced changes in mechanical properties of TiAlN/Al₂O₃ multilayers



J.Y. Yan^a, D.J. Li^{a,*}, L. Dong^{a,e}, C.K. Gao^a, N. Wang^a, X.Y. Deng^a, H.Q. Gu^{b,c}, R.X. Wan^{b,c}, X. Sun^d

^a College of Physics and Electronic Information Science, Tianjin Normal University, Tianjin 300387, China

^b Tianjin Institute of Urological Surgery, Tianjin Medical University, Tianjin 300070, China

^c Ninth People's Hospital, Shanghai Jiao Tong University, School of Medicine, Shanghai 200011, China

^d Department of Mechanical and Materials Engineering, University of Western Ontario, London, ON, Canada

^e Key Laboratory of Beam Technology and Material Modification of Ministry of Education, Beijing Normal University, Beijing 100875, China

ARTICLE INFO

Article history:

Received 1 September 2012

Received in revised form 10 November 2012

Accepted 18 November 2012

Available online 21 January 2013

Keywords:

Magnetron sputtering
TiAlN/Al₂O₃ multilayer
Modulation structure
Wear
Hardness

ABSTRACT

TiAlN/Al₂O₃ multilayers which had different separate layer thickness of TiAlN or Al₂O₃ were synthesized by sputtering Ti₃Al and Al₂O₃ targets with N₂ and Ar gases. The influence of modulation periods and modulation ratios on structure and properties of TiAlN/Al₂O₃ multilayers was investigated using scanning electron microscopy, X-ray diffraction, X-ray Photoelectron Spectroscopy, surface profiler, and nanoindenter. Compared to TiAlN layer with only (200) preferred orientation, TiAlN/Al₂O₃ multilayers were crystallized with orientations in the TiAlN (111), TiAlN (222) and AlN (100). Besides, weak Al₂O₃ (022) orientation is observed, when modulation period is 8.9 nm. The maximum hardness about 36.6 GPa was obtained at modulation period of 10.4 nm and modulation ratio of 10:1. The hardness and the toughness of TiAlN/Al₂O₃ multilayers increase as individual TiAlN layer thickness increases.

© 2013 Elsevier B.V. All rights reserved.

1. Introduction

Hard coatings have been widely used to enhance the performance and the lifetime of cutting tools in industrial applications. As is well-known, TiAlN is relatively excellent coating material due to its high hardness, wear, chemical inertness and superior oxidation resistance [1,2]. It is a good method to improve the mechanical properties of TiAlN coating further by the incorporation of other materials and by microstructure control. For the TiAlN based nano-structured coatings, such as (Ti, Cr, Al)N/(Al, Si)N, the mechanical properties were reported to be much superior to those of TiAlN coating [3].

In the last two decades, the multi-element systems have received more attention to further improving the performance [4]. A lot of multilayers of nitride/nitride, nitride/carbide, nitride/boride, such as TiN/TiAlN [5], TiAlSiN/Si₃N₄ [6], TiAlN/TiB₂ [7], TiB₂/BN [8], synthesized by Physical Vapor Deposition (PVD) have been investigated. But, nitride/oxide multilayered systems had a few reports. Pronounced strength enhancement, optimal hardness/toughness ratios and excellent wear resistance can be obtained through a proper bilayer thickness design for nanoscale multilayers [9–11].

In addition, many researchers used N₂ and Ar mixed gas as the reactive media [12].

In this work, TiAlN/Al₂O₃ multilayers with different separate layer thickness of TiAlN or Al₂O₃ were synthesized by sputtering Ti₃Al and Al₂O₃ targets with N₂ and Ar gases. The effect on layer structure, orientation, element concentrations, mechanical and wear properties of multilayers were studied.

2. Material and methods

TiAlN/Al₂O₃ multilayers with different modulation periods (A) and modulation ratios $t_{\text{TiAlN}}/t_{\text{Al}_2\text{O}_3}$ were deposited on Si (100) substrate at a fixed substrate bias of -60 V by magnetron sputtering. First of all, Si (100) substrates were cleaned in an ultrasonic agitator in acetone and ethanol for 15 min and dried using compressed air after each cleaning cycle. Subsequently, after the substrates were sputter-cleaned by -500 V Ar⁺ ion for 5 min, the deposition of the multilayers started with the deposition of 80 nm-thick TiAlN buffer layer to improve coating adhesion. High purity Ti₃Al (99.99%) target and Al₂O₃ (99.99%) target were, respectively connected to RF source sputter guns, which were installed with the horizontal plane. The substrates paralleled to the targets surface with a vertical distance of 7 cm to the target. The chamber was evacuated to a base pressure lower than 4.0×10^{-4} Pa. Then, the TiAlN/Al₂O₃ multilayers were synthesized in a flowing N₂ + Ar

* Corresponding author.

E-mail address: dejunli@mail.tjnu.edu.cn (D.J. Li).

gas mixture with N_2/Ar ratio being kept at 1/10 and the working pressure was kept at 0.4 Pa. All the depositions were conducted using a power of 100 W for the Ti_3Al target and Al_2O_3 target. The thickness of the layer was controlled by the open time of baffle and calculated by multiplying the deposition rate by the sputtering time. To determine the deposition rate, $TiAlN$ and Al_2O_3 individual layer were firstly deposited for 1 h, respectively and then the thickness of the individual layers was measured by a surface profiler, and the deposition rate thus can be calculated. As a result, layer thickness in multilayers can be calculated by multiplying the deposition rate by the sputtering time. Respectively, the deposition rates of $TiAlN$ and Al_2O_3 are about 250 and 50 nm/h. Total thickness of multilayers is about 600 nm.

The cross-section image of the multilayers was observed by a field-emission scanning electron microscopy (SEM, Hitachi 4800, Japan). A D/MAX 2500 diffractometer was used for low-angle X-ray reflectivity (XRR) and wide angle X-ray diffraction (XRD) of layered structure and crystalline analysis, operating with $Cu K\alpha$ radiation at 1.54056 Å. Residual stress (σ) generated during the coating growth process was calculated by applying Stoney formula [13] according to the measured curvature using an XP-2 profiler: $\sigma = \frac{E_s t_s^2}{6t_c(1-\nu_s)R}$ where E_s , t_s and ν_s were respectively elastic modulus, thickness and poisson ratio of the substrate, t_c the coating thickness, and R the radius of curvature of the multilayer coated substrate. The variation in the concentrations of the main elements with depth of the multilayers was analyzed by X-ray Photoelectron Spectroscopy (XPS, PHI 5300 ESCA, USA). The hardness and the elastic modulus of the multilayers were investigated by the continuous stiffness measurement (CSM) technique using a Nano Indenter XP system. This system was also used to perform scratch test.

3. Results and discussion

Clear peaks are observed in XRR patterns for the $TiAlN/Al_2O_3$ multilayers, as shown in Fig. 1(a). This indicates that periodic layers and sharp interfaces between two individual layers are formed in the $TiAlN/Al_2O_3$ multilayers as shown in the below cross-sectional SEM image. The XRR patterns give information on the Λ of the multilayers. The Λ is calculated by the modified Bragg's equation [14]: $\sin^2 \theta_n = \left(\frac{n\lambda}{2\Lambda}\right)^2 + 2\delta$, where n is the ordinal number of reflection peak, $\lambda = 1.54056$ Å is the X-ray wavelength, and δ is the correct value which is related to the average reflective index. Using equation above, three different Λ are calculated by the slope of linear least-squares fitted straight line of $\sin^2 \theta_n$ versus n^2 which is shown in the inserted figure. They are 5.8, 7.1 and 10.4 nm. The calculated $\Lambda = 10.4$ nm is nearly agreement with practical modulation period value in the cross-sectional SEM observation. Fig. 1(b) gives direct information of a well-defined composition modulation and layer structure from the $TiAlN/Al_2O_3$ multilayer. The dark layer is Al_2O_3 and the light layer is $TiAlN$. This observation of about 10 ± 1 nm- Λ is very close to our calculated values of 10.4 nm.

The XPS main element depth profile of this multilayer is shown in Fig. 2. It is obvious that the highest Ti and the lowest Ti compare the lowest Al and the highest Al, respectively. The periodic variation of the concentrations of main metal Ti and Al in the opposite tendency with the depth increasing gives a direct evidence of the multilayered modulation, implying the formation of alternating $TiAlN$ and Al_2O_3 layers.

XRD patterns of $TiAlN/Al_2O_3$ multilayers with different Λ at a constant $t_{TiAlN}:t_{Al_2O_3}$ of 10:1 and individual layers of both Al_2O_3 and $TiAlN$ are shown in Fig. 3. Al_2O_3 layer is observed as amorphous phase, whereas $TiAlN$ layer shows the strong polycrystalline with $TiAlN(200)$ preferred orientation. When Al_2O_3 layers are periodic incorporated into $TiAlN$ layer, the strong $TiAlN(200)$ texture vanishes. It indicates that Al_2O_3 layers block the growth of

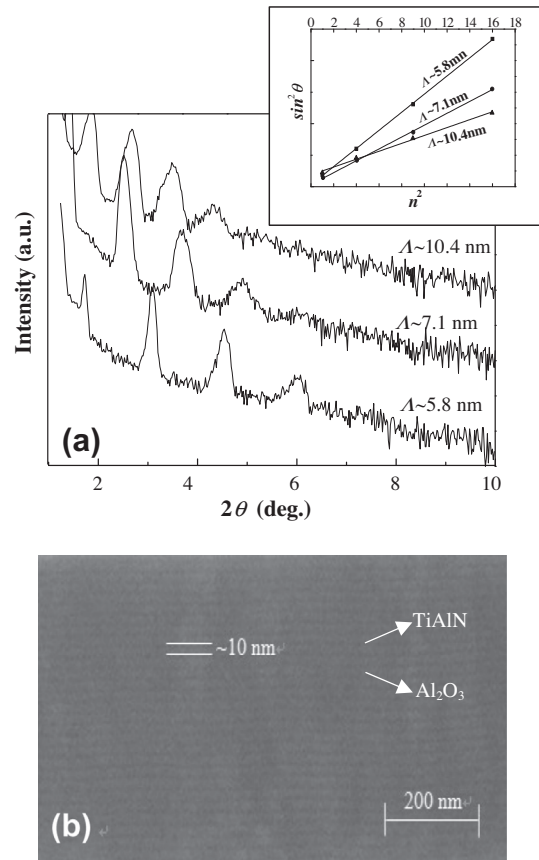


Fig. 1. (a) Low angle XRR patterns for $TiAlN/Al_2O_3$ multilayers with different Λ ; (b) Cross-sectional SEM images of $TiAlN/Al_2O_3$ multilayer with $\Lambda \sim 10$ nm.

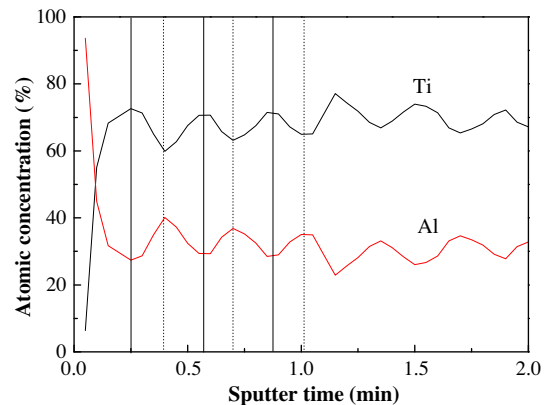


Fig. 2. A XPS main element depth profile in the cross-section of $TiAlN/Al_2O_3$ multilayer.

$TiAlN(200)$ orientation. $TiAlN/Al_2O_3$ multilayers are crystallized with orientations in the $TiAlN(111)$, $TiAlN(222)$ and $AlN(100)$. Meanwhile, with increasing Λ , $TiAlN(111)$ and (222) textures become weaker at first and then stronger. A stronger $TiAlN(111)$ and (222) peak are found in $\Lambda = 14.2$ nm. Besides, weak $Al_2O_3(022)$ orientation is observed, when Λ is 8.9 nm.

Fig. 4 shows the variations of hardness and elastic modulus as a function of Λ at a constant $t_{TiAlN}:t_{Al_2O_3} = 10:1$ together with hardness and elastic modulus of $TiAlN$ and Al_2O_3 individual layers. With increasing Λ , the hardness of the multilayers decreases before increases. When Λ is more than 7.1 nm, the hardness is higher than that of $TiAlN$ individual layers. The maximum hardness of 36.6 GPa

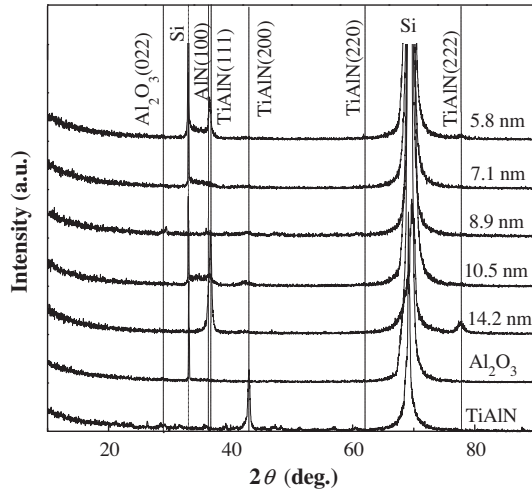


Fig. 3. XRD patterns for monolithic coatings and TiAlN/Al₂O₃ multilayers with different λ .

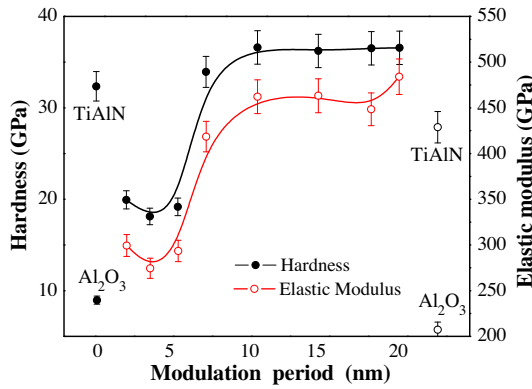


Fig. 4. Hardness and elastic modulus of TiAlN/Al₂O₃ multilayers with different λ .

is obtained at $\lambda = 10.4$ nm. The change of elastic modulus is similar to one of hardness. The nature of the nanoscale multilayered modulation and interfaces is critical to the variation of hardness, because sharp TiAlN/Al₂O₃ interfaces and proper modulation period can restrain dislocations from gliding and columnar grains from growing across layers [15]. According to hardness formula of $H = \lambda_a H_a / \lambda + \lambda_b H_b / \lambda$ (H_a and H_b are hardness of TiAlN and Al₂O₃ individual layers, λ_a and λ_b represent thickness of TiAlN and Al₂O₃ layers in a multilayer, respectively, λ is total thickness of a multilayer), hardness and elastic modulus of the multilayer at $t_{\text{TiAlN}}:t_{\text{Al}_2\text{O}_3} = 10:1$ should be 30.2 and 409 GPa. However, real hardness and elastic modulus of our multilayer at $t_{\text{TiAlN}}:t_{\text{Al}_2\text{O}_3} = 10:1$ are higher 6.4 and 53 GPa than the theoretical value. Some researches discussed several possible explanations for the hardness behavior, including the supermodulus effect, coherency strains, and grain size reduction [16–18]. In this work, a possible mechanism influencing hardness and elastic modulus is that the incorporation of Al₂O₃ blocks growth of TiAlN grains and motion of dislocations or defects in the individual layers.

Fig. 5 shows the effect of $t_{\text{TiAlN}}:t_{\text{Al}_2\text{O}_3}$ on hardness and elastic modulus at a constant $\lambda = 10$ nm. Hardness of the TiAlN/Al₂O₃ multilayers increases firstly and then decreases with decreasing $t_{\text{TiAlN}}:t_{\text{Al}_2\text{O}_3}$. In contrast, it is obvious that thicker Al₂O₃ layer or thinner TiAlN layer may induce TiAlN layer to become partially amorphous and hence softer. The maximum hardness is up to 36.6 GPa in the case of $\lambda = 10$ nm and $t_{\text{TiAlN}}:t_{\text{Al}_2\text{O}_3} = 10:1$ which

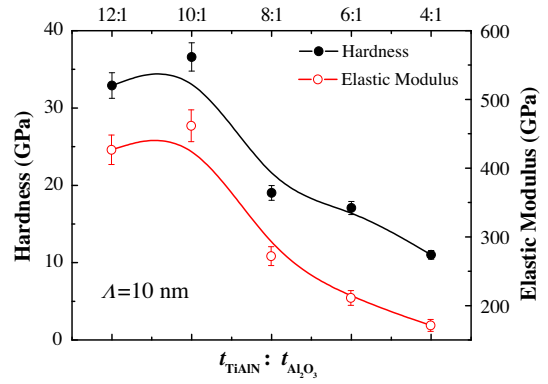


Fig. 5. Hardness and elastic modulus of TiAlN/Al₂O₃ multilayers with different $t_{\text{TiAlN}}:t_{\text{Al}_2\text{O}_3}$.

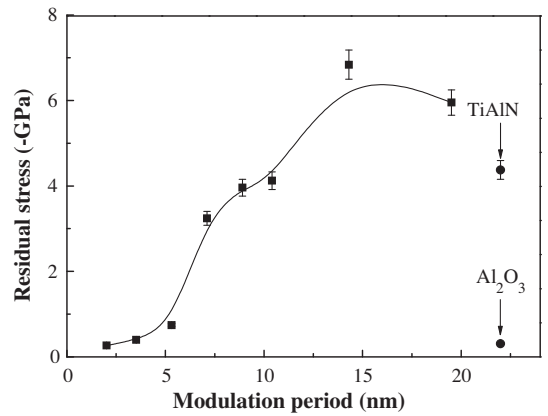


Fig. 6. Residual stress of TiAlN/Al₂O₃ multilayers at different λ .

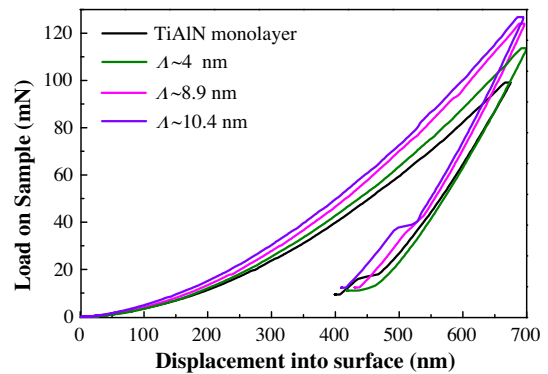


Fig. 7. Typical load vs nano-indenter displacement curve of TiAlN/Al₂O₃ multilayers with different λ and TiAlN monolayer.

are the best condition. Lowest hardness (11 GPa) and elastic modulus (172 GPa) approach to Al₂O₃ monolayer. Elastic modulus is also similar to hardness. It indicates that increasing Al₂O₃ layer block polycrystalline with TiAlN coatings.

The residual stress, i.e. compressive stress of the multilayers determined by XP-2 profiler is influenced by λ as is shown in Fig. 6. It is known that residual stress is generated during the coating growth process. High residual stress (σ) is the main reason for coating delamination and plastic deformation. Therefore, the reduced residual stress in coatings is a key factor for these coatings to explore more applications. With increasing λ , the stress of the

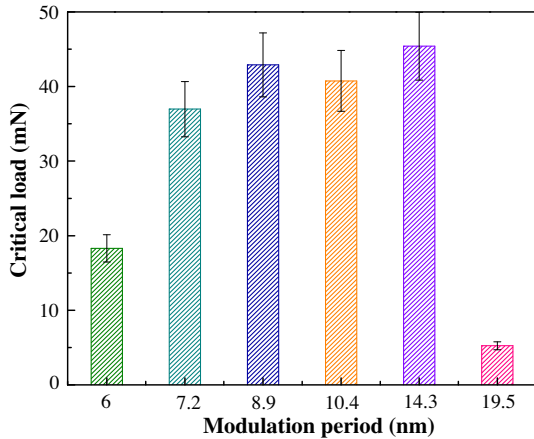


Fig. 8. The critical fracture load of TiAlN/Al₂O₃ multilayers with different λ .

multilayers increases. Multilayers with modulation periods less than 10 nm have lower compressive stress than the value of TiAlN individual layers. It is due to periodically introduction of Al₂O₃ layers into TiAlN layers that helps to relax the stress built in TiAlN layers.

The typical loading-unloading curves of TiAlN/Al₂O₃ multilayers with two different λ at a constant $t_{\text{TiAlN}}:t_{\text{Al}_2\text{O}_3} = 10:1$ and TiAlN individual layer are shown in Fig. 7. Obviously, when pressed same displacement into surface, larger λ need larger load. Compared to TiAlN monolayer, TiAlN/Al₂O₃ multilayers at $\lambda = 8.9$ nm and $\lambda = 10.4$ nm have stronger plastic recovery, because its area surrounded by loading-unloading curve is smaller than others. To the contrary, the multilayer with a λ of 4 nm displays weaker plastic recovery due to Al₂O₃ layer.

Fig. 8 shows the critical fracture load of TiAlN/Al₂O₃ multilayers with different λ . The normal load corresponding to an abrupt increase point in the scratch scan profile is the critical fracture load of coatings (L_c). The L_c can characterize the adhesion strength of the coating or the coating's fracture resistance. The coating's fracture resistance may be also interrelated with inherent internal stress, hardness, and plastic recovery. The L_c of monolithic TiAlN coating is 21 mN. With increasing λ , the L_c value tends gradually to maximum and then decreases. The multilayers between 8.9 and 14.3 nm have higher L_c value. Their values are all over 40 mN, indicating the best fracture resistance among all coatings. This indicates that well fracture resistance appears to be directly related to high hardness and strong plastic recovery of the coating with multilayered structure.

4. Conclusion

In the study, multilayer TiAlN/Al₂O₃ multilayers and monolayer TiAlN and Al₂O₃ coatings are synthesized by a magnetron sputtering system. TiAlN/Al₂O₃ multilayers are crystallized with orientations in the TiAlN (111), TiAlN (200), TiAlN (222) and AlN (100). The Al₂O₃ monolayer with thicker thickness would block the grain growth of TiAlN to form nanocrystals in the multilayers. The mechanical properties of TiAlN/Al₂O₃ multilayers are directly bound up with the Al₂O₃ monolayer thickness. The maximum hardness and elastic modulus about 36.6 and 462 GPa of the multilayers occur at the modulation period of 10.4 nm and the modulation ratio of 10:1. Meanwhile, the critical fracture load of TiAlN/Al₂O₃ multilayers reaches highest value. Our results indicate that TiAlN/Al₂O₃ multilayers appear to be a promising multilayer system suitable for engineering applications.

Acknowledgements

This work was supported by National Basic Research Program of China (973 Program, 2012CB933600), National Natural Science Foundation of China (51272176, 11075116).

References

- [1] A. Hörling, L. Hultman, M. Odén, J. Sjölen, L. Karlsson, Surf. Coat. Technol. 191 (2005) 384–389.
- [2] K. Chu, Y.G. Shen, W.-D. Münz, Vac. J. Sci. Technol. A21 (1986) 2717–2721.
- [3] N. Fukmoto, H. Ezura, K. Yamamoto, A. Hotta, T. Suzuki, Surf. Coat. Technol. 203 (2009) 1343–1348.
- [4] J.L. Endrino, S. Palacin, M.H. Aguirre, A. Gutiérrez, F. Schäfers, Acta Mater. 55 (2007) 2129–2134.
- [5] Yongqiang wei, Chunzhi Gong, Appl. Surf. Sci. 257 (2011) 7881–7886.
- [6] K. Zhang, L.S. Wang, G.H. Yue, Y.Z. Chen, D.L. Peng, Z.B. Qi, Z.C. Wang, Surf. Coat. Technol. 205 (2011) 3588–3595.
- [7] Y.D. Sun, J.Y. Yan, S. Zhang, F.Y. Xue, G.Q. Liu, D.J. Li, Vacuum 86 (2012) 949–952.
- [8] L. Dong, D.J. Li, S. Zhang, J.Y. Yan, M.Y. Liu, C.K. Gao, N. Wang, G.Q. Liu, H.Q. Gu, R.X. Wan, Thin Solid Films 520 (2012) 5328–5332.
- [9] U. Helmersson, S. Todorova, S.A. Barnett, J.-E. Sundgren, L.C. Markert, J.E. Greene, J. Appl. Phys. 62 (1987) 481–487.
- [10] X. Chu, S.A. Barnett, J. Appl. Phys. 77 (1995) 4403–4409.
- [11] P.C. Yashar, W.D. Sproul, Vacuum 55 (1999) 179–190.
- [12] S.S. Zhao, H. Du, J.D. Zheng, Y. Yang, W. Wang, J. Gong, C. Sun, Surf. Coat. Technol. 202 (2008) 5170–5174.
- [13] M. Ohring, The Material Science of Thin Films, Academic Press, San Diego, 1992.
- [14] V. Holý, T. Baumbach, Phys. Rev. B 49 (1994) 10668–10676.
- [15] J.S. Koehler, Phys. Rev. B2 (1970) 547–551.
- [16] A. Madan, Y. Wang, S.A. Barnett, C. Engstrom, H. Ljungcrantz, L. Hultman, M. Grimsditch, J. Appl. Phys. 84 (1998) 776–782.
- [17] X. Chu, M.S. Wong, W.D. Sproul, S.A. Barnett, J. Mater. Res. 14 (1999) 2500–2508.
- [18] S.A. Barnett, A. Madan, Scr. Mater. 50 (2004) 739–744.